Catalysis Letters (2019) 149:860–869
https://doi.org/10.1007/s10562-019-02657-2

Selective and Low Overpotential Electrochemical CO_2 Reduction to Formate on CuS Decorated CuO Heterostructure

Amaha Woldu Kahsay[1] · Kassa Belay Ibrahim[2] · Meng-Che Tsai[1] · Mulatu Kassie Birhanu[1] · Soressa Abera Chala[1] · Wei-Nien Su[2] · Bing-Joe Hwang[1,3]

Received: 19 October 2018 / Accepted: 6 January 2019 / Published online: 17 January 2019

Abstract

Cu_2O/CuO/CuS electrocatalyst was prepared by thermal oxidation of cleaned copper mesh in the air into Cu_2O/CuO and CuS was deposited on oxide surface using facile successive ionic layer adsorption and reaction method. The successive fabrication of the electrocatalyst was confirmed using XRD, SEM, Raman and XPS. The catalytic enhancement is believed to be associated with the reduction of copper sulfide. Together with copper oxides, they offer favorable adsorption sites for electrochemical CO_2 reduction. The synthesized catalyst offered significantly enhanced activity and selectivity performance for CO_2 reduction at lower overpotential. Remarkably, the faradaic efficiency for formate generation reaches 84% at the potential of − 0.7 V versus RHE. It has also provided a high partial current density of − 20 mA cm^{-2}.

Graphical Abstract

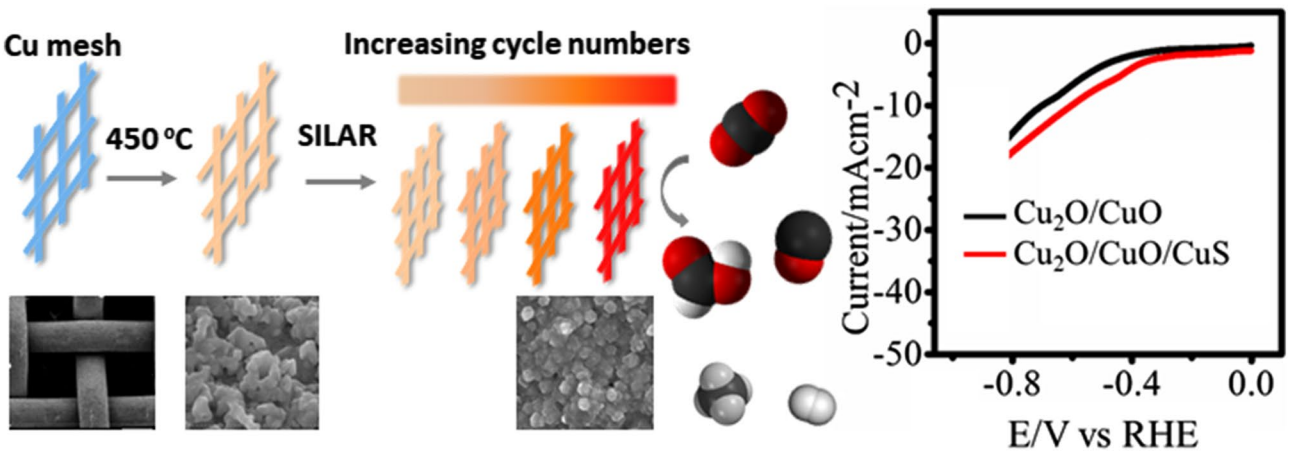

Keywords CuS · Cu_2O/CuO/CuS · Electrocatalyst · Electrochemical CO_2 reduction · SILAR method

1 Introduction

The electrochemical CO_2 reduction into chemical commodities and fuels, powered by renewable energy electricity, is a fascinating approach to provide affordable clean energy, reduce our dependence on conventional fossil fuels, and mitigate the impact of climatic changes due to global warming [1–3]. However, two main challenges have prohibited CO_2 electroreduction from becoming viable technology: energy

Electronic supplementary material The online version of this article (https://doi.org/10.1007/s10562-019-02657-2) contains supplementary material, which is available to authorized users.

✉ Wei-Nien Su
wsu@mail.ntust.edu.tw

✉ Bing-Joe Hwang
bjh@mail.ntust.edu.tw

Extended author information available on the last page of the article

inefficiency due to high overpotential requirement and poor selectivity leading to post separation processes.

Since the ground-breaking work by Hori et al., the 1980s, wide range of bulk metals have been explored as an electrocatalyst for CO_2 reduction [4]. Based on the main product distribution, they are categorized as formate forming (Pb, Sn, Hg, Tl, In), carbon monoxide forming (Au, Ag, Zn), hydrogen forming (Fe, Pt, Ni, Mo,) and hydrocarbon forming (Cu) metal catalysts.

Copper is the only metal that can electrochemically convert CO_2 into hydrocarbons. It reduces CO_2 to a wide spectrum of hydrocarbon products such as methane, ethylene, methanol, ethanol and propanol [5]. However, its fast deactivation during electrolysis, poor selectivity and high overpotential requirements limit its practical applications. Recent studies have focused on nanostructured electrocatalyst to improve catalytic activities and selectivity. Over the past several years, different types of nanostructured copper electrocatalyst have been explored for CO_2 reduction including nanoparticles [6, 7], nanowires [8–10]. Significant improvements have been also made by forming alloys with transition metals like Cu-Au [11, 12], Cu-Ag [13], Cu-Pd [14], Cu-Pt [15], and post transition metals such as Cu-Sn [16], Cu-In [17]. Metal catalysts derived from the corresponding oxide have currently been identified as a promising CO_2 electroreduction catalyst. Their synthesis method involves anodization, thermal oxidation of the metal substrate in the air or electrodeposition followed by in situ electrochemical reductions or annealing under hydrogen atmosphere to obtain oxide derived catalysts.

Kanan et al. [18] synthesized copper electrocatalyst by thermal oxidation of copper foil in the air and electrochemically reduced the Cu_2O films. The oxide derived catalyst showed improved catalytic activity which relies on the initial thickness of Cu_2O films. The same group described structural properties of the metallic component, derived from the in situ reductions during the CO_2 conversion process [19, 20]. Such reduction of the metallic oxide into the metallic phase is because of the applied cathodic potential for CO_2 activation. Furthermore, Kas et al. [21] Studied the CO_2 reduction on copper nanoparticles derived from electrodeposited Cu_2O with different orientations ([110][111] [100]). The authors indicated that the thickness of the initial Cu_2O layer strongly influenced the product selectivity than the initial crystal orientation of Cu_2O, which agrees with the previous study on OD-Cu [18]. Smith et al. [22] prepared copper nanowire catalyst via two-step synthesis of $Cu(OH)_2$ and CuO nanowires on copper foil and electrochemically reduced into copper nanowires during CO_2 electrolysis. Remarkable improvements in catalytic activity and selectivity were obtained and the catalytic performances were related to the binding strength of the catalyst to $COOH^*$ intermediates. Wang et al. [8] synthesized CuO nanowires on Cu mesh by thermal oxidation in air and then reduced into Cu nanowires by using two reduction methods (under a hydrogen atmosphere or applying a cathodic electrochemical potential) for comprative analysis. The two reduction methods produced Cu nanowires with similar dimensions but different surface structures and the Cu nanowires produced by electrochemical reduction were extremely active and selective for CO_2 reduction, realizing faradaic efficiency around 60% CO production. Additionally, the same group developed copper nanowires from CuO nanowires by tuning the reduction temperature and heating time under a hydrogen atmosphere. The optimized Cu nanowires exhibited superior performance and selectivity. The faradaic efficiency of CO production increased to 65% and of ethanol the production as high as 50% at potentials more positive than −0.5 V (versus reversible hydrogen electrode, RHE) [23]. The selectivity of oxide derived copper catalysts is dependent on structural morphology and copper oxidation state [21, 24–29]. Grain boundaries, local pH, and surface roughness, under coordinated sites are other factors which promote activity, selectivity and stability [30, 31]. On the other hand, there are research reports that described the catalytic role of subsurface oxide species in the surface region, [24, 32]. However, the presence of Cu^+ species and stability during electrochemical CO_2 reduction is still the subject of debate [33]. Recently, Sargent et al. [34] synthesized copper catalyst with controlled morphology and oxidation states from a sol–gel using electro-redeposition, the dissolution and redeposition of copper, to enhance copper catalytic performance. The authors reported that in situ X-ray spectroscopy and density functional theory simulations results showed the advantageous of both sharp morphologies and Cu^+ oxidation state for super ethylene production. However, still paramount efforts and further improvements in terms of catalyst stability and selectivity and reducing overpotentials of CO_2 reduction are required. Therefore, there is an increasing emphasis on the development of efficient, selective and affordable electrocatalysts for CO_2 conversion. Recently, transition metal chalcogenides (TMCs) have attracted scientists' attention because of their promising applications in energy storages and electrocatalysis of hydrogen evolution reactions [35]. Their low cost and high earth abundance are other important benefits of these materials. However, there are limited reports on their applications in CO_2 electroreduction [36, 37], Sn(S)/Au [38] and CuS [39].

As mentioned above, the oxidized metals can be utilized as a precursor for the preparation of the completely reduced metal phase catalyst or partially oxidized species which might be able to survive during CO_2 conversion and serve as a catalyst. However, the fast copper oxide reduction during electrochemical CO_2 reduction remains a challenging problem. Considering this challenge and the promising activities of sulfides for CO_2, here we synthesized three dimensional

copper oxide heterostructure modified by CuS to minimize copper oxide reduction and promote catalytic activity of copper sulfide on the surface using simple and facile method for electrochemical CO_2 reduction in aqueous solution. There are different types of film production method such as magnetron spattering, sol–gel processes, electrodeposition and chemical bath deposition methods to deposit co-catalyst. In this work, we used successive ionic layer adsorption reaction (SILAR) method to deposit CuS on to thermally prepared Cu_2O/CuO heterostructure. This method does not require vacuum at any stage of the process. It can be carried out at ambient conditions. Moreover, the deposition kinetics and the thickness of the film can be easily managed by changing the number of deposition cycles.

2 Experimental Part

2.1 Electrocatalyst Preparation Methods

2.1.1 Cu_2O/CuO Synthesis

Cu_2O/CuO was prepared using thermal oxidation on the pre-treated copper mesh. Briefly, the copper mesh was pretreated using 0.1 M HCl, DI water and acetone and dried under argon purging. The hetrostructured oxides were developed on the copper mesh by annealing in a cubic furnace in air at 450 °C for 4 h.

2.1.2 CuS Deposition

CuS was deposited on Cu_2O/CuO using simple and scalable successive ionic layer adsorption and reaction (SILAR) method adopted from our group's pervious work [40]. Cu_2O/CuO/Cu mesh was immersed in 0.01 M $Cu(NO_3)_2$ methanol solution and subsequently in 0.01 M Na_2S methanol solution at room temperature for 1 min each. After each immersion, the electrode was rinsed using pure methanol to remove excess adsorbed ions and residues from the precursors. The amount of CuS deposited was controlled by the number of SILAR cycles (immersion and rinsing). Samples are denoted as Cu_2O/CuO/CuS-x, where x indicates the number of applied SILAR cycles.

2.2 Characterization of Electrocatalyst

X-ray diffraction analysis was performed using a Bruker D2 phase XRD − 300W machine, equipped with a Cu-Kα irradiation photon source (λ = 1.5406 Å, Ni filter, 40 kV, and 100 mA) at a range of 10–80°. All samples are analyzed at room temperature in the 2θ range of 10°–80°, with a scanning speed of 0.1° s^{-1} and 0.05°/step. The morphological of the synthesized films were performed using scanning electron microscopy (SEM) images and energy dispersive X-ray (EDX) analysis. The image was taken with a Hitachi S-4700 microscope using an accelerating voltage of 15 kV. Raman patterns of all nanocatalysts were performed on a UniRAM micro-Raman spectrometer integrated by Protrustech Co., Ltd. A solid-state laser with λ = 532 nm was used as the excitation source with a laser power of 20 mW to avoid degradation with 10 s exposure time and 15 accumulations. X-ray photoelectron spectroscopy (XPS) measurments were carried out at National Taiwan University, Taiwan with 24 A XPS beamline station and wide-range beamline (BL24A). All reported binding energies were corrected using the signal for the carbon peak (C 1 s) at 284.5 eV.

2.3 Electrochemical Reduction of CO_2 and Product Analysis

H-shaped three-electrode electrochemical cell was used, where Pt wire, Ag/AgCl(saturated KCl) were used as counter and reference electrodes respectively. The anodic and cathodic compartments were separated by a Nafion memberane. Both compartments were filled with 60 ml of 0.1 M $KHCO_3$ aqeous electrolyte. The counter electrode was connected to the anode compartment while reference and working electrodes were connected to the cathode compartment. Argon gas was purged to the solution for 30 min to remove air. The electrocatalyst surface was cleaned by using cyclic votammetry at scan rate 20 mVs^{-1}. Finally, pure CO_2 gas was purged in the cathode compartment for 30 min and the pH of the electrolyte was maintained at 6.8 when electrochemical measurments were performed. The linear sweepvoltammetry was measured in the potential range from − 1.2 to 0.0 V versus RHE both Ar -saturated and CO_2-saturtated 0.1 M $KHCO_3$ solution at the scan rate of 10 mVs^{-1}. The potentials measured were converted to the reversible hydrogen electrode (RHE) reference scale by using $E_{RHE} = E_{Ag/AgCl} + 0.197 + 0.059$ x pH.

Electrochemical setup was integrated with gas chromatography to quantify gaseous products. The schematic diagram of GC coupled with the electrochemical system is shown in Figure S2. During the electrolysis, CO_2 was constantly purged into the cathodic compartment at a rate of 20.0 mL per min controlled by a mass flow controller and vented directly into the gas chromatograph (GC) (ACME6100, Vastech Instruments). The GC has equipped with a packed Parapak N, 60/80 mesh, leftx1/8″ column and Molecular Sieve 5A, 80/100 mesh, 6fitx1/8″. Helium gas was used as the carrier gas. The pulsed discharge helium ionization detector (PDHID) was used to quantify inorganic (H_2, CO), and organic CH_4, C_2H_4 and C_2H_6, gas products. The GC measurements were recorded every 30 min for three times and the average of the three measurements was used in the data analysis.

Liquid products were analyzed on a 500 MHz NMR spectrometer (Bruker Avance). 2 ml of electrolyte (0.1 M $KHCO_3$ aqueous) was taken by syringe from cathode compartment of the electrochemical reactor after CO_2 electrolysis for 2.5 h and mixed in 0.1 ml of 5 mM dimethyl sulfoxide. Then 0.5 ml the mixture were taken and mixed in 0.7 ml D_2O (99.9%, Cambridge Isotope Lab), and then transferred to NMR sample tube. The 1D 1H spectra were measured with water suppression by a pre-saturation technique. The liquid product concentrations were calculated with reference to an internal standard (dimethyl sulfoxide).

3 Results and Discussion

3.1 Catalyst Synthesis

Cu_2O/CuO /CuS catalyst was prepared on the commercially available copper mesh using scalable and simple two- step synthesis processes as shown in Scheme 1. During the first thermal oxidation, Cu_2O/CuO layers were formed on the surface of the copper mesh and then copper sulfide nanoparticles were loaded on it by SILAR of Cu_2O/CuO electrode in 0.01 M methanol solutions of copper nitrate and sodium sulfide. The thermal oxidation of copper mesh and the experimental set-up of the manually operated SILAR deposition system are illustrated in Scheme 1. That is, clean copper mesh (Scheme 1a) was firstly oxidized in air (at 450 °C for 4 h) to fabricate the electrode (Scheme 1b). Then Cu_2O/ CuO was dipped in the cationic precursor solution ($Cu(NO_3)_2$) for 1 min, resulting in Cu^{2+} being adsorbed onto the surface of the Cu_2O/CuO film (Scheme 1c). Consequently, this electrode was immersed in methanol solution for 10 s to remove excess adsorbed ions from the precursor (Scheme 1d). Thirdly, the sample was then immersed in the anionic precursor (Na_2S) solution for 1 min, resulting in the reaction of sulfide ions (S^{2-}) with the adsorbed Cu^{2+} on the surface of the Cu_2O/CuO electrode (Scheme 1e). Lastly, the excess and/or unreacted species and the reaction byproduct from the diffusion layer were removed by rinsing the electrode in pure methanol solution (Scheme 1f). Through this, one cycle of CuS deposition on the surface of Cu_2O/CuO layer was completed. The amount deposited CuS can be increased and controlled by repeating the immersion cycles.

3.2 Physical Characterization of the Catalyst

The XRD patterns of bare Cu_2O/CuO /Cu-mesh and Cu_2O/CuO modified with CuS are displayed in Fig. 1a. The diffraction peaks at 43.4°, 50.6°, and 74.4° are characteristic for copper metal with corresponding facets in (111), (200) and (220). With annealing treatment, Cu-mesh resulted in the formation of CuO and Cu_2O species, as indicated by peaks at 35.5°, 38.8° and 39.15°(JCPDS Card No. 5-661) corresponding to CuO (002), (111), and (200); and at 29.7°, 36.6°, 42.3°, 61.3° and 73.99° (JCPDS Card No. 05-0667) which correspond to (110), (111), (200), (220) and (311) facets of Cu_2O.

The presence of mixed oxides in the annealed Cu arises from the formation of CuO/Cu_2O composite indicating that

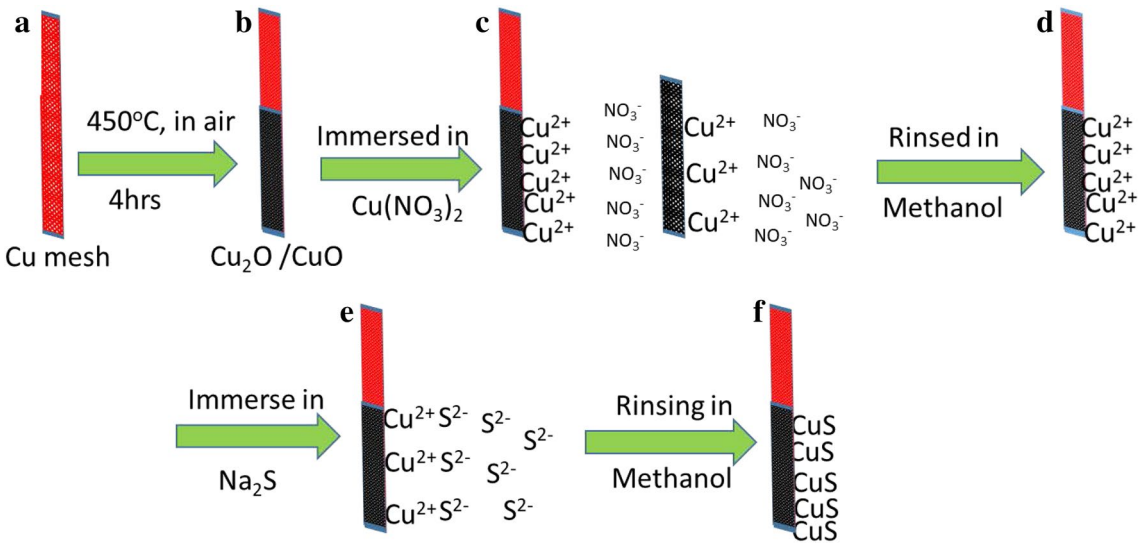

Scheme 1 Illustration of thermal oxidation and SILAR growth: **a** Copper mesh before thermal oxidation, **b** Cu_2O/CuO grown on copper mesh, **c** adsorption of Cu^{2+} and $NO^-{}_3$ and the formation of an electrical double layer, **d** rinsing (I) removes excess unabsorbed Cu^{2+} and NO_3^-, **e** reaction of S^{2-} with pre-adsorbed Cu^{2+} ions to form CuS, and **f** rinsing (II) to remove excess and unreacted species and form the solid solution CuS on surface of the Cu mesh/Cu_2O/CuO

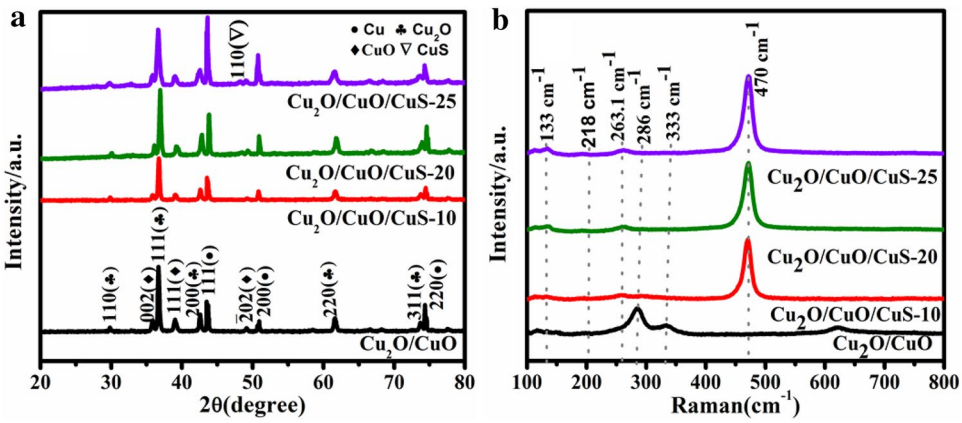

Fig. 1 **a** XRD patterns and **b** Raman spectra of Cu_2O/CuO and after CuS deposition on Cu_2O/CuO for 10, 20 and 25 SILAR cycles

temperature and time applied for heat-treatment was not high enough for complete oxidation of Cu_2O species to CuO [40]. This confirms the formation of cubic Cu_2O and monoclinic CuO nanostructures on the copper mesh surfaces. The XRD pattern with CuS coated oxide also displayed a similar pattern to that of copper oxide, indicating the copper sulfide layer generated by SILAR deposition was not detectable enough by XRD at low deposition cycles. However, at high deposition cycles (Cu_2O/CuO/CuS-20) new peak appeared at 48.1° (JCPDS Card No. 65–393) with the corresponding reflection of (110). Surface sensitive Raman spectroscopic technique was employed for further conformation and Raman spectra were obtained as displayed in Fig. 1b. The strong peak at (286, 333, and 623) and a weak peak at 218 cm^{-1} can be assigned to CuO and Cu_2O constituents of the heterostructure of bare Cu_2O/CuO respectively. Raman spectra of Cu_2O/CuO modified electrode indicate new peaks at 133, 263.1 and 190 cm^{-1}. The strong peak at 470 cm^{-1} attributed to the vibrational mode of S–S bond stretching. The peaks assigned to oxides disappeared with further SILAR deposition cycle increases which confirm the successful deposition of CuS.

For further confirmation, we performed scanning electron microscopy (SEM) measurements on bare and modified electrocatalysts at different cycles were performed. The bare copper mesh is presented in Fig. 2a and as-prepared Cu_2O/

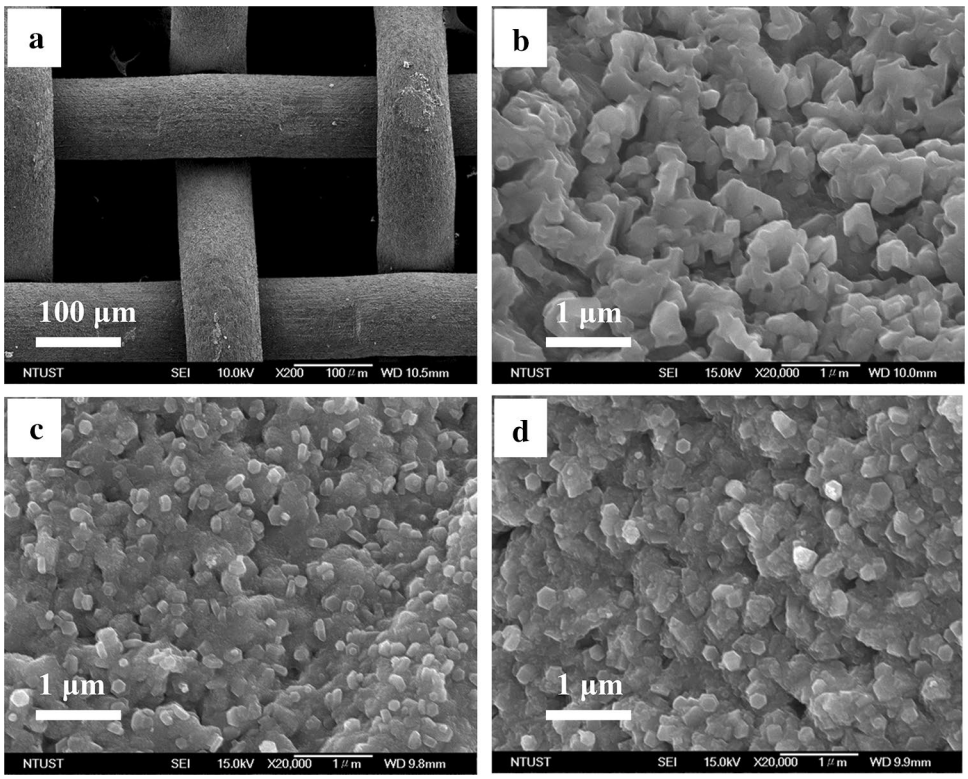

Fig. 2 Scanning electron microscopy images of **a** bare copper mesh, **b** Cu_2O/CuO, **c** Cu_2O/CuO/CuS-10, and **d** Cu_2O/CuO/CuS-20

CuO shown in Fig. 2b exhibits a crystalline feature. After modifications, the oxide surface is covered by increasing CuS deposition, as SILAR deposition number increases. The energy-dispersive X-ray (EDX) spectrum (Fig. S1) also supports that the Cu_2O/CuO/CuS electrocatalyst consists of copper, oxygen and sulfur elements with the different atomic ratio depending on the deposition cycles. From the analysis of Raman scattering and EDX, we are able to confirm the successful deposition of CuS by SILAR method.

XPS analysis was carried out to investigate the elemental composition of Cu_2O/CuO and Cu_2 O/CuO/CuS-20. Figure 3a displays survey spectra of Cu_2O/CuO and Cu_2O/CuO/CuS-20. Cu_2 O/CuO sample contains peaks characteristic of Cu 2p, O 1 s, and C 1 s. However, the Cu_2O/CuO/CuS-20 has an additional peak that corresponds to S 2p. The weak peaks of C could be from the adventitious hydrocarbon of the XPS instrument itself. The main peaks located at 933.6 and 953.7 eV (Fig. 3b) for Cu_2O/CuO were assigned to Cu $2p_{3/2}$ and Cu $2p_{½}$ respectively. Additionally, there were satellite peaks at around 943 eV and 962.2 eV. In the case of the XPS spectrum of Cu 2p for Cu_2O/CuO/CuS-20, the Cu $2p_{3/2}$ and Cu $2p_{1/2}$ peaks were observed at 932.2 and 952.2 eV (Fig. 3b), respectively. Moreover, there are weak satellite peaks at around 943 eV signifying the presence of the paramagnetic chemical state of Cu^{2+} [41]. The corresponding XPS spectrum of O 1 s is indicated in Fig. 3c. The binding energy peaks indicated in the S 2p spectrum at 162.0 and 163.1 eV (Fig. 3d), which are related to the S $2p_{3/2}$ and S $2p_{1/2}$, confirms the successful deposition of CuS on top of copper oxides.

3.3 Electrocatalytic Performance for CO_2 Reduction

Before measuring electrochemical performance, the catalyst was reduced using chronoamperometry by applying constant potential for 50 min. During this reduction processes, the color of the Cu_2O/CuO film changed from black to light orange indicating a reduction of oxides to copper nanoparticle on the copper mesh. However, after SILAR modification, no color change was observed. This implies the oxide surface was covered by CuS. The catalytic performance of bare Cu_2O/CuO and CuS modified electrocatalyst was evaluated by linear sweep voltammetry (LSV) in Argon and CO_2 saturated 0.1 M $KHCO_3$ aqueous solutions in a three-electrode system respectively. As shown in Fig. 4a, bare Cu_2O/CuO displays similar current density curves in both Ar saturated and CO_2 saturated solutions. However, the current density of CuS- modified electrocatalyst show significant improvement

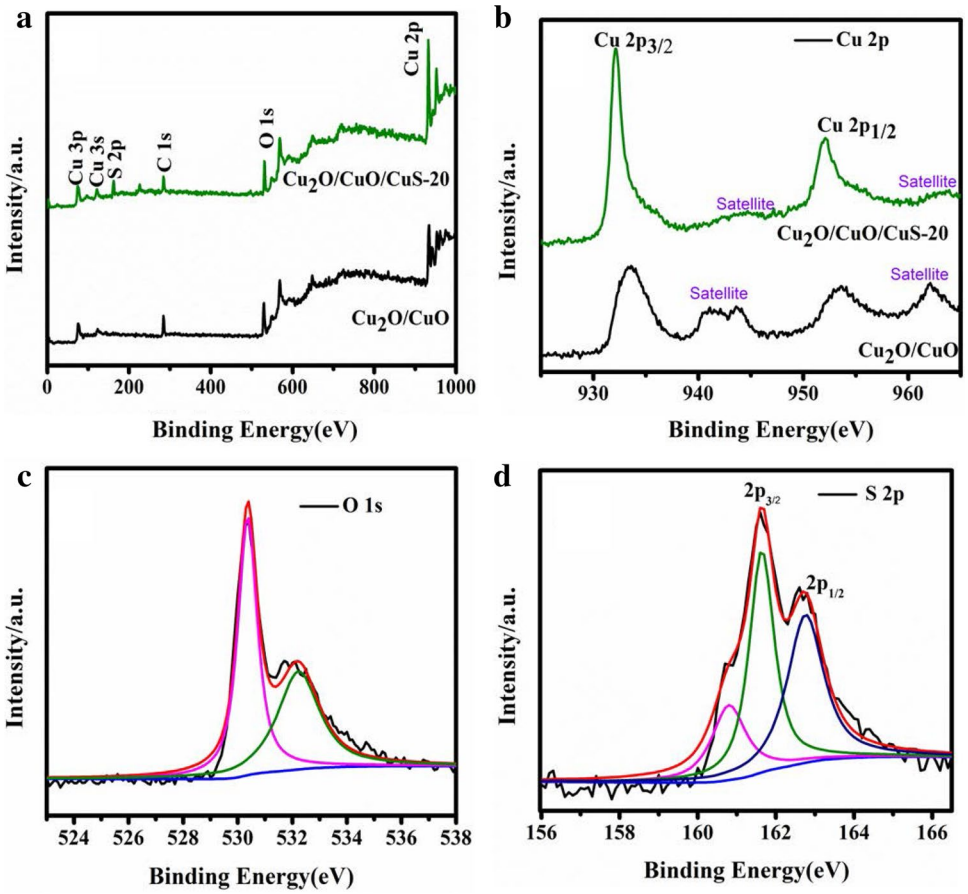

Fig. 3 **a** XPS survey spectra of Cu_2O/CuO and Cu_2O/CuO/CuS-20, **b** the Cu 2p region of the XPS spectra of Cu_2O/CuO and Cu_2O/CuO/CuS-20, **c** XPS O 1 s spectrum of Cu_2O/CuO, and **d** XPS S 2p spectrum of Cu_2O/CuO/CuS-20

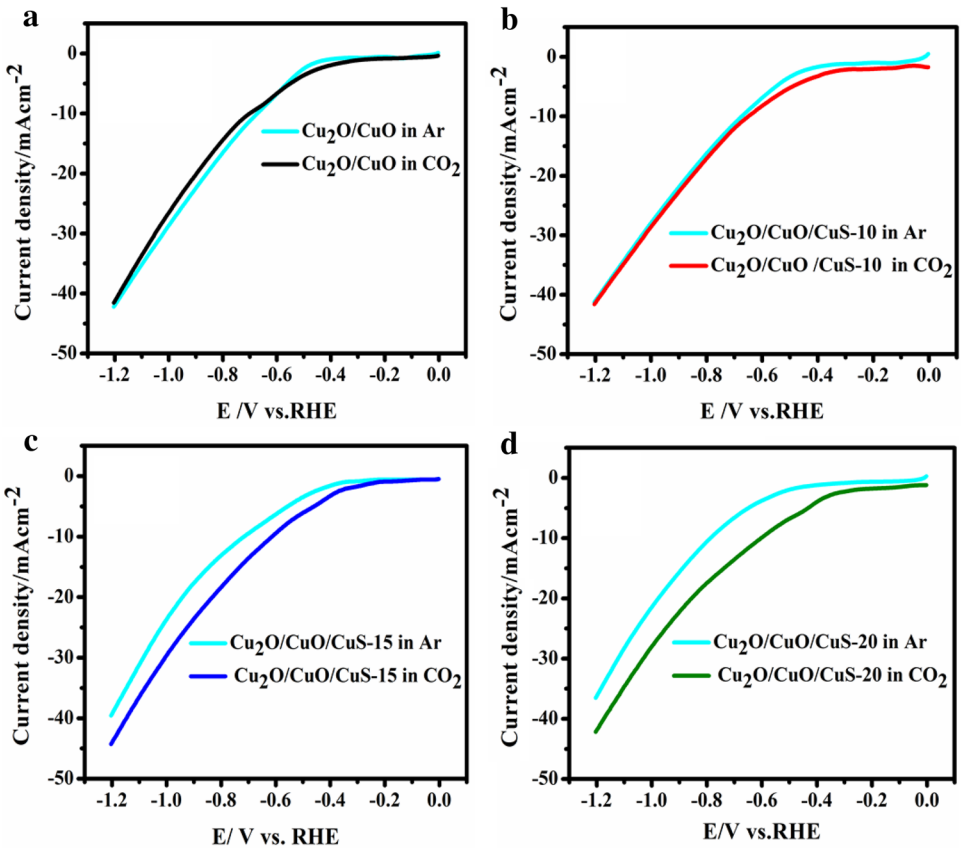

Fig. 4 Linear sweep voltammetry of **a** Cu_2O/CuO, **b** Cu_2O/CuO/CuS-10, **c** Cu_2O/CuO/CuS-15 and **d** Cu_2O/CuO/CuS-20 in Ar saturated and CO_2 saturated 0.1 M $KHCO_3$ electrolytes at a scan rate of 10 mV s^{-1}

in CO_2 saturated $KHCO_3$ solution compared with Ar saturated solution showing that the modified catalyst can reduce CO_2 in $KHCO_3$ aqueous solution.

As seen in Fig. 4b–d, selectivity increases with increasing the number of deposition cycles. Significant improvements have been observed at low overpotentials ranging from − 0.8 to − 0.4 V. Moreover, the onset potential for CO_2 reduction by Cu_2O/CuO/CuS-20 has improved to − 0.22 V in CO_2 saturated $KHCO_3$ solution compared with Ar- saturated solution indicating that the catalyst has enhanced electrochemical CO_2 reduction abilities at low overpotentials.

Furthermore, product distribution and stability of the catalysts were investigated. For this purpose we have selected copper sulfide coated (Cu_2O/CuO/CuS-20) and bare Cu_2O/CuO at selected reduction potential, i.e. − 0.7 V versus RHE. Detailed product analysis was performed on these two catalysts to quantify the gas and liquid products using gas chromatography and NMR respectively. Under this applied potential range, hydrogen and formate were detected in a significant amount. Representative spectra of NMR and gas chromatography at selected potential are illustrated in Fig. 5a, b. Formate was found to be the main liquid product by Cu_2O/CuO/CuS-20, while hydrogen was still the main (side) products in gas phase. In Fig. 5c, CuS deposition by the SILAR method proves to successfully passivate Cu_2O/CuO and reduce or retard the corrosion.

The modified catalyst demonstrated dramatically increased performance and selectivity for formate formation and suppressed hydrogen evolution. The bare electrode has low faradaic efficiency for formate (22%), while generating a significant amount of hydrogen (68%). In contrary, a highest faradaic efficiency of formate (84%) was achieved at the modified catalyst with significantly suppressed hydrogen generation with faradaic efficiency of around 17%. A high formate partial current density of 20 mA cm^{-2} together with faradaic efficiency of 84% was reached on Cu_2O/CuO/CuS-20. The catalyst performance is significantly increased compared with some selected electrocatalysts reported in the literature, as summarized in Table 1.

The catalytic enhancement could be attributed by the partial electrochemical reduction of copper sulfide into copper nanoparticles. It is also believed that the reduced sulfur can create some steric hindrance and thus may weaken the binding strength of $COOH^*$ intermediate and favor the pathway for formate formation [42]. Together with the copper oxides, a catalytic synergy is created in the composite and more favorable adsorption sites are generated for facilitating the electrochemical CO_2 reduction.

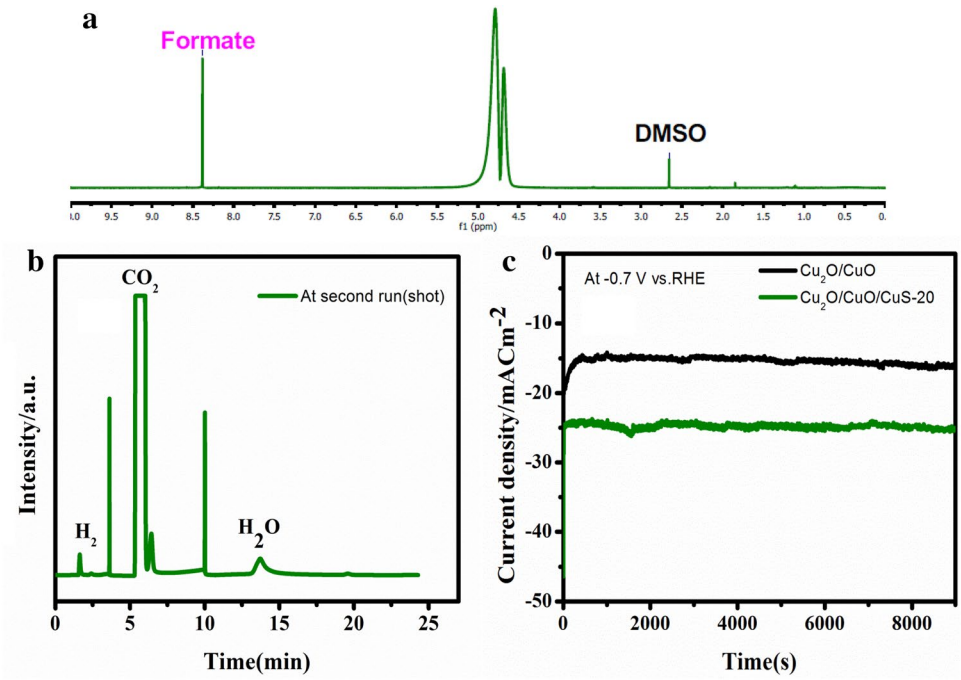

Fig. 5 **a** NMR spectrum of the 0.1 M $KHCO_3$ catholyte after 2.5 h of CO_2 electrolysis on Cu_2O/CuO/CuS-20. Potential applied: − 0.7 V versus RHE. **b** Gas chromatogram recorded during electrochemical CO_2 reduction by Cu2O/CuO/CuS-20 at applied potential of − 0.7 V versus RHE. **c** Stability test of electrochemical CO_2 reduction current as a function of electrocatalysis time for bare oxides (Cu_2O/CuO) and modified catalyst (Cu_2O/CuO/CuS-20) at − 0.7 V versus RHE for 2.50 h in 0.1 M $KHCO_3$ saturated with CO_2

Table 1 Summary of selected catalysts displaying selective conversion CO_2 to formate

Catalyst	Electrolyte	Applied potential	J_{HCOO-} (mA cm^{-2})	FE_{HCOO-} (%)	Reference
S-doped Cu_2O derived Cu	0.1 M $KHCO_3$	− 0.8 V (vs. RHE)	− 10.7	74	[42]
S-modified Cu	0.1 M $KHCO_3$	− 0.8 V (vs. RHE)	− 10	80	[39]
Nano-Sn/graphene	0.1 M $NaHCO_3$	− 1.8 V (vs. SCE)	− 9.5	94	[43]
SnS_2 derived Sn/SnS_2 nanosheet	0.5 M $NaHCO_3$	− 1.4 V (vs. Ag/AgCl)	− 11.8	85	[44]
Pd NP/C	2.8 M $KHCO_3$	− 0.15 V (vs. RHE)	− 4.2	95	[45]
Sn–Pb alloy	0.5 M $KHCO_3$	− 2.0 V (vs. Ag/AgCl)	− 45.7	79.8	[46]
Cu_2O/CuO/CuS	01. M $KHCO_3$	− 0.7 V (vs. RHE)	− 20.0	84	This work

4 Conclusions

In summary, we successfully deposited copper sulfide nanoparticles on to thermally synthesized copper oxide by simple and facile SILAR method and tested its catalytic performance for electrochemical CO_2 reduction. The modified electrocatalyst exhibited high selectivity for formate formation at low overpotential. Remarkably, maximum faradaic efficiency of 84% and enhanced partial current density of − 20 mA cm^{-2} were obtained at over potential of − 0.7 V. Copper sulfides can undergo electrochemical reduction during electrochemical CO_2 electrolysis and this can contribute to the enhanced electrocatalytic activity. Together with copper oxides, a catalytic synergy is created in the composite and more favorable adsorption sites are generated for facilitating the electrochemical CO_2 reduction. This study paves the way to controlling the composition—selectivity relationship using facile and scalable catalyst synthesis approach.

Acknowledgements Financial support was provided by the Ministry of Science and Technology (MOST) (105-3113-E-011-001-, 104-2911-I-011-505-MY2, 103-2923-E-011-004-MY3), the Ministry of Economic Affairs (MOEA) (101-EC-17-A-08-S1-183) the Top University Projects of Ministry of Education (MOE) (100H451401), and Taiwan's Deep Decarbonization Pathways toward a Sustainable Society Project (106-0210-02-11-03). Research facilities were provided by the National Synchrotron Radiation Research Center (NSRRC) and the National Taiwan University of Science and Technology (NTUST).

Author Contributions All authors are exhaustively discussed the results and involved to the final manuscript of this research. Amaha woldu Kahsay: Developed the methodology, performed experiments, investigated the process, processed the experimental data, characterized and analyzed the results, and draft the manuscript. Kassa Belay Ibrahim: Helped to perform XRD measurements and coordinate in research activities. Meng-Che Tsai: Contributed to the analysis of the results and coordinate in the research activities. Mulatu Kassie Birhanu: Worked out in technical activities such as sample preparation and activity measurements. Soressa Abera Chala: Contributed to the analysis of the results, discussion and helped graphic preparations. Wei-Nien Su: Helped in discussing the results, designed the figures, worked on the draft and revision of this manuscript, and supervised this

work. Bing-Joe Hwang: Devised and conceived the original ideas of this research, provide study materials, instruments, reagents and other tools for analysis, analyzed and discussed the results, critical revision and supervised this work.

References

1. Gao S, Lin Y, Jiao X, Sun Y, Luo Q, Zhang W, Li D, Yang J, Xie Y (2016) Partially oxidized atomic cobalt layers for carbon dioxide electroreduction to liquid fuel. Nature 529:68
2. Inoue T, Fujishima A, Konishi S, Honda K (1979) Photoelectrocatalytic reduction of carbon dioxide in aqueous suspensions of semiconductor powders. Nature 277:637
3. Dong ZD, Long LJ, Zhang QS (2016) Recent advances in inorganic heterogeneous electrocatalysts for reduction of carbon dioxide. Adv Mater (Weinheim Ger) 28:3423–3452
4. Qiao J, Liu Y, Hong F, Zhang J (2014) A review of catalysts for the electroreduction of carbon dioxide to produce low-carbon fuels. Chem Soc Rev 43:631–675
5. Kuhl KP, Cave ER, Abram DN, Jaramillo TF (2012) New insights into the electrochemical reduction of carbon dioxide on metallic copper surfaces. Energy Environ Sci 5:7050–7059
6. Reske R, Mistry H, Behafarid F, Roldan Cuenya B, Strasser P (2014) Particle size effects in the catalytic electroreduction of CO2 on Cu nanoparticles. J Am Chem Soc 136:6978–6986
7. Wang Z, Yang G, Zhang Z, Jin M, Yin Y (2016) Selectivity on etching: creation of high-energy facets on copper nanocrystals for CO_2 electrochemical reduction. ACS Nano 10:4559–4564
8. Raciti D, Livi KJ, Wang C (2015) Highly dense Cu nanowires for low-overpotential CO_2 reduction. Nano Lett 15:6829–6835
9. Ming M, Kristina D, Smith WA (2016) S.W. A., Controllable hydrocarbon formation from the electrochemical reduction of CO_2 over Cu nanowire arrays. Angew Chem Int Ed 55:6680–6684
10. Cao L, Raciti D, Li C, Livi KJT, Rottmann PF, Hemker KJ, Mueller T, Wang C (2017) Mechanistic insights for low-overpotential electroreduction of CO_2 to CO on copper nanowires. ACS Catal 7:8578–8587
11. Christophe J, Doneux T, Buess-Herman C (2012) Electroreduction of carbon dioxide on copper-based electrodes: activity of copper single crystals and copper–gold alloys. Electrocatalysis 3:139–146
12. Kim D, Resasco J, Yu Y, Asiri AM, Yang P (2014) Synergistic geometric and electronic effects for electrochemical reduction of carbon dioxide using gold–copper bimetallic nanoparticles. Nat Commun 5:4948
13. Clark EL, Hahn C, Jaramillo TF, Bell AT (2017) Electrochemical CO_2 reduction over compressively strained CuAg surface alloys with enhanced multi-carbon oxygenate selectivity. J Am Chem Soc 139:15848–15857
14. Ma S, Sadakiyo M, Heima M, Luo R, Haasch RT, Gold JI, Yamauchi M, Kenis PJA (2017) Electroreduction of carbon dioxide to hydrocarbons using bimetallic Cu–Pd catalysts with different mixing patterns. J Am Chem Soc 139:47–50
15. Varela AS, Schlaup C, Jovanov ZP, Malacrida P, Horch S, Stephens IEL, Chorkendorff I (2013) CO_2 electroreduction on well-defined bimetallic surfaces: Cu overlayers on Pt(111) and Pt(211). J Phys Chem C 117:20500–20508
16. Sarfraz S, Garcia-Esparza AT, Jedidi A, Cavallo L, Takanabe K (2016) Cu–Sn bimetallic catalyst for selective aqueous electroreduction of CO_2 to CO. ACS Catal 6:2842–2851
17. Larrazábal GO, Martín AJ, Mitchell S, Hauert R, Pérez-Ramírez J (2016) Enhanced reduction of CO_2 to CO over Cu–In electrocatalysts: catalyst evolution is the key. ACS Catal 6:6265–6274
18. Li CW, Kanan MW (2012) CO_2 reduction at low overpotential on Cu electrodes resulting from the reduction of thick Cu_2O films. J Am Chem Soc 134:7231–7234
19. Chen Y, Kanan MW (2012) Tin oxide dependence of the CO_2 reduction efficiency on tin electrodes and enhanced activity for Tin/Tin oxide thin-film catalysts. J Am Chem Soc 134:1986–1989
20. Chen Y, Li CW, Kanan MW (2012) Aqueous CO_2 reduction at very low overpotential on oxide-derived Au nanoparticles. J Am Chem Soc 134:19969–19972
21. Kas R, Kortlever R, Milbrat A, Koper MTM, Mul G, Baltrusaitis J (2014) Electrochemical CO_2 reduction on Cu_2O-derived copper nanoparticles: controlling the catalytic selectivity of hydrocarbons. Phys Chem Chem Phys 16:12194–12201
22. Ma M, Djanashvili K, Smith WA (2015) Selective electrochemical reduction of CO_2 to CO on CuO-derived Cu nanowires. Phys Chem Chem Phys 17:20861–20867
23. Raciti D, Cao L, Livi KJT, Rottmann PF, Tang X, Li C, Hicks Z, Bowen KH, Hemker KJ, Mueller T, Wang C (2017) Low-overpotential electroreduction of carbon monoxide using copper nanowires. ACS Catal 7:4467–4472
24. Mistry H, Varela AS, Bonifacio CS, Zegkinoglou I, Sinev I, Choi Y-W, Kisslinger K, Stach EA, Yang JC, Strasser P, Cuenya BR (2016) Highly selective plasma-activated copper catalysts for carbon dioxide reduction to ethylene. Nat Commun 7:12123
25. Lee S, Kim D, Lee J (2015) Electrocatalytic production of C3-C4 compounds by conversion of CO_2 on a chloride-induced bi-phasic Cu2O-Cu catalyst. Angew Chem Int Ed 54:14701–14705
26. Loiudice A, Lobaccaro P, Kamali EA, Thao T, Huang BH, Ager JW, Buonsanti R (2016) Tailoring copper nanocrystals towards C_2 products in electrochemical CO_2 reduction. Angew Chem Int Ed 55:5789–5792
27. Gao D, Zegkinoglou I, Divins NJ, Scholten F, Sinev I, Grosse P Roldan Cuenya B (2017) Plasma-activated copper nanocube catalysts for efficient carbon dioxide electroreduction to hydrocarbons and alcohols. ACS Nano 11:4825–4831
28. Chen CS, Handoko AD, Wan JH, Ma L, Ren D, Yeo BS (2015) Stable and selective electrochemical reduction of carbon dioxide to ethylene on copper mesocrystals. Catal Sci Technol 5:161–168
29. Handoko AD, Ong CW, Huang Y, Lee ZG, Lin L, Panetti GB, Yeo BS (2016) Mechanistic insights into the selective electroreduction of carbon dioxide to ethylene on Cu_2O-derived copper catalysts. J Phys Chem C 120:20058–20067
30. Feng X, Jiang K, Fan S, Kanan MW (2015) Grain-boundary-dependent CO_2 electroreduction activity. J Am Chem Soc 137:4606–4609
31. Verdaguer-Casadevall A, Li CW, Johansson TP, Scott SB, McKeown JT, Kumar M, Stephens IEL, Kanan MW, Chorkendorff I (2015) Probing the active surface sites for CO reduction on oxide-derived copper electrocatalysts. J Am Chem Soc 137:9808–9811
32. Eilert A, Cavalca F, Roberts FS, Osterwalder J, Liu C, Favaro M, Crumlin EJ, Ogasawara H, Friebel D, Pettersson LGM, Nilsson A (2017) Subsurface oxygen in oxide-derived copper electrocatalysts for carbon dioxide reduction. J Phys Chem Lett 8:285–290
33. Eilert A, Roberts FS, Friebel D, Nilsson A (2016) Formation of copper catalysts for CO_2 reduction with high ethylene/methane product ratio investigated with in situ x-ray absorption spectroscopy. J Phys Chem Lett 7:1466–1470
34. De Luna P, Quintero-Bermudez R, Dinh C-T, Ross MB, Bushuyev OS, Todorović P, Regier T, Kelley SO, Yang P, Sargent EH (2018) Catalyst electro-redeposition controls morphology and oxidation state for selective carbon dioxide reduction. Nat Catal 1:103–110
35. Yu Z, Qian Z, Jixin Z, Qingyu Y, Xue DS, Wenping S (2017) Nanostructured metal chalcogenides for energy storage and electrocatalysis. Adv Funct Mater 27:1702317

36. Zhao Z, Peng X, Liu X, Sun X, Shi J, Han L, Li G, Luo J (2017) Efficient and stable electroreduction of CO_2 to CH_4 on CuS nanosheet arrays. J Mater Chem A 5:20239–20243
37. Jiaqi X, Xiaodong L, Wei L, Yongfu S, Zhengyu J, Tao Y, Chengming W, Huanxin J, Junfa Z, Shiqiang W, Yi X (2017) Carbon dioxide electroreduction into syngas boosted by a partially delocalized charge in molybdenum sulfide selenide alloy monolayers. Angew Chem Int Ed 56:9121–9125
38. Zheng X, De Luna P, García de Arquer FP, Zhang B, Becknell N, Ross MB, Li Y, Banis MN, Li Y, Liu M, Voznyy O, Dinh CT, Zhuang T, Stadler P, Cui Y, Du X, Yang P, Sargent EH (2017) Sulfur-modulated tin sites enable highly selective electrochemical reduction of CO_2 to formate. Joule 1:794–805
39. Shinagawa T, Larrazábal GO, Martín AJ, Krumeich F, Pérez-Ramírez J (2018) Sulfur-modified copper catalysts for the electrochemical reduction of carbon dioxide to formate. ACS Catal 8:837–844
40. Dubale AA, Tamirat AG, Chen H-M, Berhe TA, Pan C-J, Su W-N, Hwang B-J (2016) A highly stable CuS and CuS-Pt modified Cu2O/CuO heterostructure as an efficient photocathode for the hydrogen evolution reaction. J Mater Chem A 4:2205–2216
41. Ye M, Wen X, Zhang N, Guo W, Liu X, Lin C (2015) In situ growth of CuS and Cu1.8S nanosheet arrays as efficient counter electrodes for quantum dot-sensitized solar cells. J Mater Chem A 3:9595–9600
42. Huang Y, Deng Y, Handoko AD, Goh GKL, Yeo BS (2018) Rational design of sulfur-doped copper catalysts for the selective electroreduction of carbon dioxide to formate. ChemSusChem 11:320–326
43. Zhang S, Kang P, Meyer TJ (2014) Nanostructured tin catalysts for selective electrochemical reduction of carbon dioxide to formate. J Am Chem Soc 136:1734–1737
44. Li F, Chen L, Xue M, Williams T, Zhang Y, MacFarlane DR, Zhang J (2017) Towards a better Sn: efficient electrocatalytic reduction of CO2 to formate by Sn/SnS2 derived from SnS2 nanosheets. Nano Energy 31:270–277
45. Min X, Kanan MW (2015) Pd-catalyzed electrohydrogenation of carbon dioxide to formate: high mass activity at low overpotential and identification of the deactivation pathway. J Am Chem Soc 137:4701–4708
46. Choi SY, Jeong SK, Kim HJ, Baek I-H, Park KT (2016) Electrochemical reduction of carbon dioxide to formate on Tin–lead alloys. ACS Sustain Chem Eng 4:1311–1318

Affiliations

Amaha Woldu Kahsay[1] · Kassa Belay Ibrahim[2] · Meng-Che Tsai[1] · Mulatu Kassie Birhanu[1] · Soressa Abera Chala[1] · Wei-Nien Su[2] · Bing-Joe Hwang[1,3]

[1] Nano-Electrochemistry Laboratory, Department of Chemical Engineering, National Taiwan University of Science and Technology, Taipei 106, Taiwan, Republic of China

[2] Nano-Electrochemistry Laboratory, Graduate Institute of Applied Science and Technology, National Taiwan University of Science and Technology, Taipei 106, Taiwan, Republic of China

[3] National Synchrotron Radiation Research Center, Hsin-chu, Taiwan, Republic of China